A thermalized electrokinetics model including stochastic reactions suitable for multiscale simulations of reaction-advection-diffusion systems

Ingo Tischler, Florian Weik, Robert Kaufmann,
Michael Kuron, Rudolf Weeber, and Christian Holm
Institute of Computational Physics, University of Stuttgart, Germany

(Dated: July 24, 2021)

Abstract

We introduce a scheme to simulate the spatial and temporal evolution of the densities of charged species, taking into account diffusion, thermal fluctuations, coupling to a carrier fluid, and chemical reactions. To this end, the diffusive fluxes in the electrokinetic model by Capuani *et al.* [1] are supplemented with thermal fluctuations. Chemical reactions are included via an additional source term in the mass balance equation. The diffusion-reaction model is then coupled to a solver for fluctuating hydrodynamics based on the lattice Boltzmann method. We describe our implementations, one based on the automatic code generation tools using pystencils and lbmpy, and another one contained as in the molecular dynamics package ESPResSo which allows the coupling of particles to the density fields. We validate our implementations by demonstrating that the expected influence of density fluctuations on the reaction rate for chemical reactions of order > 1 is reproduced. Our novel algorithm will be applicable to coarse-grained catalysis problems as well as to many other multi-scale problems that require the coupling of explicit-particle simulations with flow fields, diffusion, and reaction problems in arbitrary geometries.

I. INTRODUCTION AND HISTORY

The lattice electrokinetics model by Capuani *et al.* [1] is an advection-diffusion model for multiple species that interact electrostatically. Hydrodynamic effects are taken into account by means of the lattice Boltzmann method [2–4]. The model is applicable in those cases where effects on the level of the individual ion can be neglected and the system can be described by continuous density fields. Since the lattice Boltzmann method can easily handle any geometry as long as it is resolved on the grid, suitable applications are found in research fields ranging from the transport of electrolytes through porous media to biomolecules and colloids in solutions containing ions [5–7], as well as the investigation of microfluidic mechanisms like pumps [8] or selective particle traps [9, 10]. An extension of the electrokinetic model to moving colloids in binary fluid flows is also available [11].

The electrokinetic model can be extended to include chemical reactions by adding source terms to the mass balance equation [12]. These lead to the conversion of different species into each other as governed by the reaction rates. In this way, the model can be used to analyse diffusion or flow-driven reactions [13] and to simulate active particles [14].

The standard electrokinetic model does not include thermal fluctuations. While this is not an issue for many applications that treat systems on larger scales, e.g. in the field of microfluidics, in some cases the fluctuations will play an important role. These include fluctuation induced instabilities [15], pattern formation [16, 17], stochastic processes in cell biology [18], transport properties [19, 20], and many processes that happen on the nanoscale where large fluctuations are present. For chemical reactions, thermal fluctuations can have a significant impact on the reaction rate if the order of the reaction is not 1: the presence of thermal fluctuations will accelerate or slow down these reactions [21]. Lastly, fluctuations in the electrokinetic model have to be taken into account when coupling it to other thermalized models, such as a fluctuating lattice Boltzmann method [22, 23] or a particle-based simulation in which the particles undergo Brownian motion. If the electrokinetic solver would not include thermal fluctuations, it would act as an energy sink, continually drawing energy from the other coupled thermalized models.

To overcome these limitations, Dean [24] added a stochastic fluctuation term to the flux in the electrokinetic equations, which can be used in combination with different models like charged dissipative particle dynamic [25] or the fluctuating immersed boundary method

[26]. In the present article, we combine the above methods to arrive at a coupled solver for fluctuating electrokinetics, fluctuating hydrodynamics, and chemical reactions. We discuss two implementations of the method. One is based on automatic code generation using pystencils [27] and lbmpy [28] that allows for fast prototyping of these models. The other one is part of the molecular dynamics software package ESPResSo [29]. This implementation, including the lattice Boltzmann method, has the advantage of being GPU-accelerated [30]. It shall also serve as the basis for future work on coupling colloidal particles subject to Brownian motion.

The paper is structured as follows: in section II we give a detailed description of the model. In section III we discuss the discretization scheme. In section IV we go into detail concerning the implementations. Section V describes how our implementations are validated. We conclude with a summary and outlook in section VI.

II. THE ELECTROKINETIC MODEL

In this section, we will first present a summary of the electrokinetic model and then describe how one can introduce thermal fluctuations. The electrokinetic model describes the diffusion and advection behaviour of N species, in the following indexed by k. The density of each species as a function of position and time is denoted by $n_k(\vec{r}, t)$. The corresponding density fluxes are $\vec{j}_k(\vec{r}, t)$.

A. Athermal model

The flux has two contributions, diffusion and advection:

$$\vec{j}_k = \vec{j}_k^{\text{diff}} + \vec{j}_k^{\text{adv}}. \tag{1}$$

We require mass conservation

$$\frac{\partial n_k}{\partial t} = -\nabla \cdot \vec{j}_k. \tag{2}$$

To obtain the diffusive contribution, we write down the free energy as a functional of density

$$F\left[n_k(\vec{r})\right] = \sum_k \underbrace{k_{\mathrm{B}} T n_k(\vec{r}) \left(\log\left(\Lambda_k^3 n_k(\vec{r})\right) - 1\right)}_{\text{ideal gas contribution}} + \underbrace{q_k n_k(\vec{r}) \Phi(\vec{r})}_{\text{electrostatics}} \tag{3}$$

with the Boltzmann constant k_{B}, temperature T, de Broglie wavelength Λ, charge of a particle q_k and the electrostatic potential Φ. The chemical potential μ_k is obtaining by taking the functional derivative of the free energy with respect to particle number:

$$\mu_k(\vec{r}) = \frac{\delta F\left[n_k\right]}{\delta n_k}. \tag{4}$$

This allows us to write the diffusive flux as

$$j_k^{\mathrm{diff}} = -\nu_k n_k \nabla \mu_k, \tag{5}$$

where ν_k is the mobility of species k. We thus have

$$\begin{aligned} \vec{j}_k^{\mathrm{diff}} &= -k_{\mathrm{B}} T \nu_k \nabla n_k - \nu_k q_k n_k \nabla \Phi \\ &= -D_k \nabla n_k - \nu_k q_k n_k \nabla \Phi. \end{aligned} \tag{6}$$

$D_k = \nu_k k_{\mathrm{B}} T$ is the diffusion coefficient fulfilling the Einstein-Smoluchowski relation . In summary, the diffusive flux consists of Fickian diffusion and of an electrostatic driving force.

Let us now consider the advective flux. It is due to the motion of the solvent fluid. At the same time, forces on the immersed species lead to a driving force on the fluid. Assuming that we work at low Reynolds number, this can be captured via the Stokes equations

$$\eta \vec{\nabla}^2 \vec{u} = \nabla p + \vec{f}, \tag{7}$$

$$\vec{\nabla} \cdot \vec{u} = 0. \tag{8}$$

Here, η is viscosity, $\vec{u}$ flow velocity, p the pressure and $\vec{f}$ a driving force density. We assume that any force acting on the immersed species is transferred instantly onto the fluid, hence

$$\vec{f} = -\sum_k \left(k_{\mathrm{B}} T \nabla n_k + q_k n_k \nabla \Phi\right) = \sum_k \frac{1}{\nu_k} \vec{j}_k^{\mathrm{diff}}. \tag{9}$$

Similarly, we assume that the immersed species move with exactly the same velocity as the underlying fluid, neglecting any inertial effects. Hence, the advective flux is

$$\vec{j}_{\mathrm{adv}} = n_k \vec{u} \tag{10}$$

The electrostatic potential is obtained by solving the Poisson equation

$$\Delta \Phi = \frac{1}{\epsilon} \sum_k q_k n_k = -4\pi l_{\mathrm{B}} k_{\mathrm{B}} T \sum_k q_k n_k \tag{11}$$

where $l_{\mathrm{B}} = \frac{e^2}{4\pi\epsilon k_{\mathrm{B}} T}$ is the Bjerrum length with ϵ being the dielectric permittivity of the solvent.

Chemical reactions can be incorporated into eq. (2) by adding a source term

$$R_k = s_k \gamma = s_k K \prod_i n_i^{\alpha_i}, \tag{12}$$

to the right-hand side. It contains the reaction rate γ, which is expressed in terms of the reaction constant K and the stoichiometric coefficients $\vec{s} = \{-a, -b, \ldots, c, d, \ldots\}$. The latter come from the chemical reaction equation $a\mathrm{A} + b\mathrm{B} + \cdots \leftrightharpoons c\mathrm{C} + d\mathrm{D} + \ldots$. The α_i define the reaction order, stating how much the reaction rate depends on the concentration of the different species, and for most chemical reactions the order of the educt species is $i \in \{\text{educts}\}, \alpha_i = s_i$, while the reaction does not depend on the product concentration and hence $i \in \{\text{products}\}, \alpha_i = 0$.

B. Thermal fluctuations

To introduce thermal fluctuations for the fluxes, we begin with the over-damped Langevin equation for N particles experiencing a single-particle potential $\psi(r)$,

$$\dot{\vec{r}}_i(t) = \vec{\eta}_i(t) - \vec{\nabla}_i \psi(\vec{r}_i, t), \tag{13}$$

where $\eta_i(t)$ is an uncorrelated Gaussian random force obeying

$$\langle \eta_i^\mu(t) \eta_j^\nu(t') \rangle = 2D\delta_{ij}\delta_{\mu\nu}\delta(t - t'), \quad \langle \vec{\eta}_i(t) \rangle = 0 \tag{14}$$

with the superscripts indicating Cartesian components.

Following ref. 24 we will derive an equation for the global density

$$n(\vec{r}, t) = \sum_{i=1}^{N} n_i(\vec{r}, t) = \sum_{i=1}^{N} \delta(\vec{r}_i(t) - \vec{r}), \tag{15}$$

where $n_i(\vec{r}, t) = \delta(\vec{r}_i(t) - \vec{r})$ is the density function of a single particle i.

With f being an arbitrary function, the definition of the single particle density $n_i(\vec{r}, t)$ allows us to write

$$f(\vec{r}_i(t)) = \int_{\mathbb{R}^3} \mathrm{d}^3 r \, n_i(\vec{r}, t) f(\vec{r}). \tag{16}$$

With this defined we can now analyse the difference of the classical and the stochastic time derivative which will lead us to a continuous time derivative of n. The classical derivative of f is

$$\frac{\mathrm{d}}{\mathrm{d}t} f(\vec{r}_i) = \int\limits_{\mathbb{R}^3} \mathrm{d}^3 r \, \frac{\partial n_i(\vec{r},t)}{\partial t} f(\vec{r}). \tag{17}$$

For the stochastic Itô derivative [31] of f, we expand equation 16 over the next time step δt. To do this we utilize Itô's lemma for a function $f(B_t, t)$ with a Brownian process B_t:

$$\mathrm{d}f = \left(\frac{\partial f}{\partial t} + \vec{\mu}_t \frac{\partial f}{\partial x} + \frac{\sigma_t^2}{2}\frac{\partial^2 f}{\partial x^2}\right)\mathrm{d}t + \sigma_t \frac{\partial f}{\partial x}\mathrm{d}B_t. \tag{18}$$

Here, $\vec{\mu}_t$ is the drift velocity and σ_t is the variance of the Brownian process. The time derivative of the Brownian process is given by $\dot{\vec{B}}_t = \vec{\eta}(t)/\sqrt{2\gamma k_\mathrm{B} T}$. With this we obtain

$$\begin{aligned}\frac{\mathrm{d}f(\vec{r}_i)}{\mathrm{d}t} &= \underbrace{\frac{\partial f}{\partial t}}_{=0} + \vec{\nabla}_i f(r_i)\left(\vec{\mu}_t + \sigma_t \frac{\mathrm{d}\vec{B}_t}{\mathrm{d}t}\right) + \frac{\sigma_t^2}{2}\nabla_i^2 f(r_i) \qquad (19)\\ &= \int \mathrm{d}^3 r f(\vec{r})\Big(\vec{\nabla}_i \cdot (n_i(\vec{r},t)\vec{\eta}_i(t)) \\ &\quad -\vec{\nabla}_i(n_i(\vec{r},t)) \cdot \vec{\nabla}_i \psi(\vec{r}_i,t) + D\nabla_i^2 n_i(\vec{r},t)\Big). \qquad (20)\end{aligned}$$

Subtracting the classical (equation 17) from the stochastic derivative (equation 20) and summing over all particles i, we arrive at

$$\frac{\partial n(\vec{r},t)}{\partial t} = \xi(\vec{r},t) - \vec{\nabla} \cdot (n(\vec{r},t)\nabla\psi(\vec{r},t)) + D\nabla^2 n(\vec{r},t), \tag{21}$$

where the noise term $\xi(\vec{r},t)$ is redefined as

$$\xi(\vec{r},t) = \sum_{i=1}^{N} \vec{\nabla} \cdot (n_i(\vec{r},t)\eta_i(t)) \tag{22}$$

to contain $n_i(\vec{r},t)$. This redefined noise term has the correlation function

$$\langle \xi(\vec{r},t)\xi(\vec{r}\,',t')\rangle = 2D\delta(t-t')\sum_{i=1}^{N} \vec{\nabla}_r \cdot \vec{\nabla}_{r'}(n_i(\vec{r},t)n_i(\vec{r}\,',t)). \tag{23}$$

The correlation function can be rewritten using the properties of the Dirac delta function yielding

$$\langle \xi(\vec{r},t)\xi(\vec{r}\,',t')\rangle = 2D\delta(t-t')\vec{\nabla}_r \cdot \vec{\nabla}_{r'}(\delta(\vec{r}-\vec{r}\,')n(\vec{r},t)). \tag{24}$$

We want to express the noise term 22 without the usage of a summation. To that end we define a different noise field, which is statistically identical. This is achieved by having the same correlation function. The new global noise field with that exact property turns out to be

$$\xi'(\vec{r},t) = \vec{\nabla} \cdot (\vec{\eta}(\vec{r},t)\sqrt{n(\vec{r},t)}) \tag{25}$$

with the global white noise field $\vec{\eta}$ characterized by

$$\langle \eta^{\mu}(\vec{r},t)\eta^{\nu}(\vec{r}\,',t')\rangle = 2D\delta^{\mu\nu}\delta(t-t')\delta(\vec{r}-\vec{r}\,'), \quad \langle \vec{\eta}(\vec{r},t)\rangle = 0. \tag{26}$$

With $\xi'(\vec{r},t)$ we can rewrite equation 21 as

$$\frac{\partial n(\vec{r},t)}{\partial t} = \vec{\nabla} \cdot \left(n(\vec{r},t)\nabla\psi(\vec{r},t) + D\nabla n(\vec{r},t) + \sqrt{n(\vec{r},t)}\vec{\eta}(\vec{r},t) \right). \tag{27}$$

This is a more general version of equation 6 with an additional noise term. Relating back to the electrokinetics model of sec. II A, where the electrostatic interaction is included as an external potential, and since we may have additional terms for advective flux and chemical reactions, this finally yields

$$\begin{aligned} \frac{\partial n_k}{\partial t} &= -\vec{\nabla} \cdot \vec{j}_k + s_k K \prod_i n_i^{\alpha_i}, \\ \vec{j}_k &= -D_k \nabla n_k - \nu_k q_k n_k \nabla\Phi - \sqrt{n_k}\vec{\eta}_k + n_k \vec{u}, \end{aligned} \tag{28}$$

where all symbols have been introduced before.

III. DISCRETIZATION

Let us now discretize the fluctuating electrokinetic equations such that they may be be solved numerically on a lattice. Recall that the continuous electrokinetic equations are

$$\begin{aligned} \frac{\partial n_k}{\partial t} &= -\nabla \cdot \vec{j}_k, \\ \vec{j}_k &= \underbrace{-D_k \nabla n_k}_{\vec{j}^{\mathrm{diff}}} \underbrace{-\nu_k q_k n_k \nabla\Phi}_{\vec{j}^{\mathrm{pot}}} \underbrace{-\sqrt{n_k}\vec{\eta}_k}_{\vec{j}^{\mathrm{fluc}}} \underbrace{+n_k \vec{v}}_{\vec{j}^{\mathrm{adv}}}. \end{aligned} \tag{29}$$

We will be using two regular cubic grids, one for the densities, and a second, staggered one, for the fluxes. The regular grid will store the mean density of the region in space that it covers. The flux is defined on the staggered grid, shifted by $\frac{a_i}{2}$ in all directions compared to the density grid. Here, a_i is the lattice constant in the direction i, which is defined by the grid stencil. There is some freedom in choosing the discretization scheme. Our choice was to be consistent with the thermal fluxes. Approximating $\vec{\nabla} \cdot \vec{j}_k$ with finite differences allows us to write

$$\vec{\nabla} \cdot \vec{j}_k(\vec{x}, t) \approx \sum_{i=1}^{q} \frac{1}{a_i A_0} (j_{k,i}(\vec{x} + \frac{\vec{a_i}}{2}, t) - j_{k,i}(\vec{x} - \frac{\vec{a_i}}{2}, t)), \tag{30}$$

where $\vec{a_i}$ is defines the vector to the nearest grid neighbours and $j_{k,i}$ is represents the flux to the given grid direction $\vec{a_i}$. A_0 is a normalization factor of the used grid stencil. This is needed for grids, where the fluxes are not linearly independent. For D2Q9, we get $A_{0,D2Q9} = 1 + \sqrt{2}$. For D3Q19 and D3Q27, we have $A_{0,D3Q19} = 1 + 2\sqrt{2}$ and $A_{0,D3Q27} = 1 + 2\sqrt{2} + \frac{4}{3}\sqrt{3}$, respectively. We now look at the different contributions to the flux, starting with the diffusive flux:

$$\vec{j}^{\,\mathrm{diff}}_{k,i}(\vec{x} + \frac{\vec{a_i}}{2}, t) = -D\vec{\nabla} n_k(\vec{x} + \frac{\vec{a_i}}{2}, t). \tag{31}$$

We use finite differences to approximate $\vec{\nabla} n_k(\vec{x} + \frac{\vec{a_i}}{2}, t)$, which yields

$$\vec{\nabla} n_k(\vec{x} + \frac{\vec{a_i}}{2}, t) \approx \frac{\vec{a_i}}{a_i^2}(n_k(\vec{x} + \vec{a_i}, t) - n_k(\vec{x}, t)). \tag{32}$$

The contribution of the electrostatic potential is treated in similar fashion, yielding

$$\vec{j}^{\,\mathrm{pot}}_{k,i}(\vec{x} + \frac{\vec{a_i}}{2}, t) = \nu_k q_k n_k(\vec{x} + \frac{\vec{a_i}}{2}, t) \nabla \Phi(\vec{x} + \frac{\vec{a_i}}{2}, t). \tag{33}$$

To approximate the density between the grid nodes, we use the arithmetic mean of the two adjacent nodes in the direction $\vec{a_i}$, which then yields

$$\vec{j}^{\,\mathrm{pot}}_{k,i}(\vec{x} + \frac{\vec{a_i}}{2}, t) \approx -\frac{\vec{a_i}}{a_i^2} \nu_k q_k \left(\frac{n_k(\vec{x} + \vec{a_i}, t) + n_k(\vec{x}, t)}{2} (\Phi(\vec{x} + \vec{a_i}, t) - \Phi(\vec{x}, t)) \right). \tag{34}$$

Calculating the advective flux, we rely on the assumption that the density of particles in the small volume represented by a node is homogeneous. The advective velocity displaces this volume and transfers it to neighbouring cells. Figure 1 illustrates this scheme in two dimensions.

Lastly the distribution due to the fluctuation are described as

$$\begin{aligned} \vec{j}^{\,\mathrm{fluc}}_{k,i}(\vec{x} + \frac{\vec{a_i}}{2}, t) &= \sqrt{n_k(\vec{x} + \frac{\vec{a_i}}{2}, t)} \eta_k(\vec{x} + \frac{\vec{a_i}}{2}, t) \\ &\approx \sqrt{\frac{n_k(\vec{x} + \vec{a_i}, t) + n(\vec{x}, t)}{2}} \eta_k(\vec{x} + \frac{\vec{a_i}}{2}, t). \end{aligned} \tag{35}$$

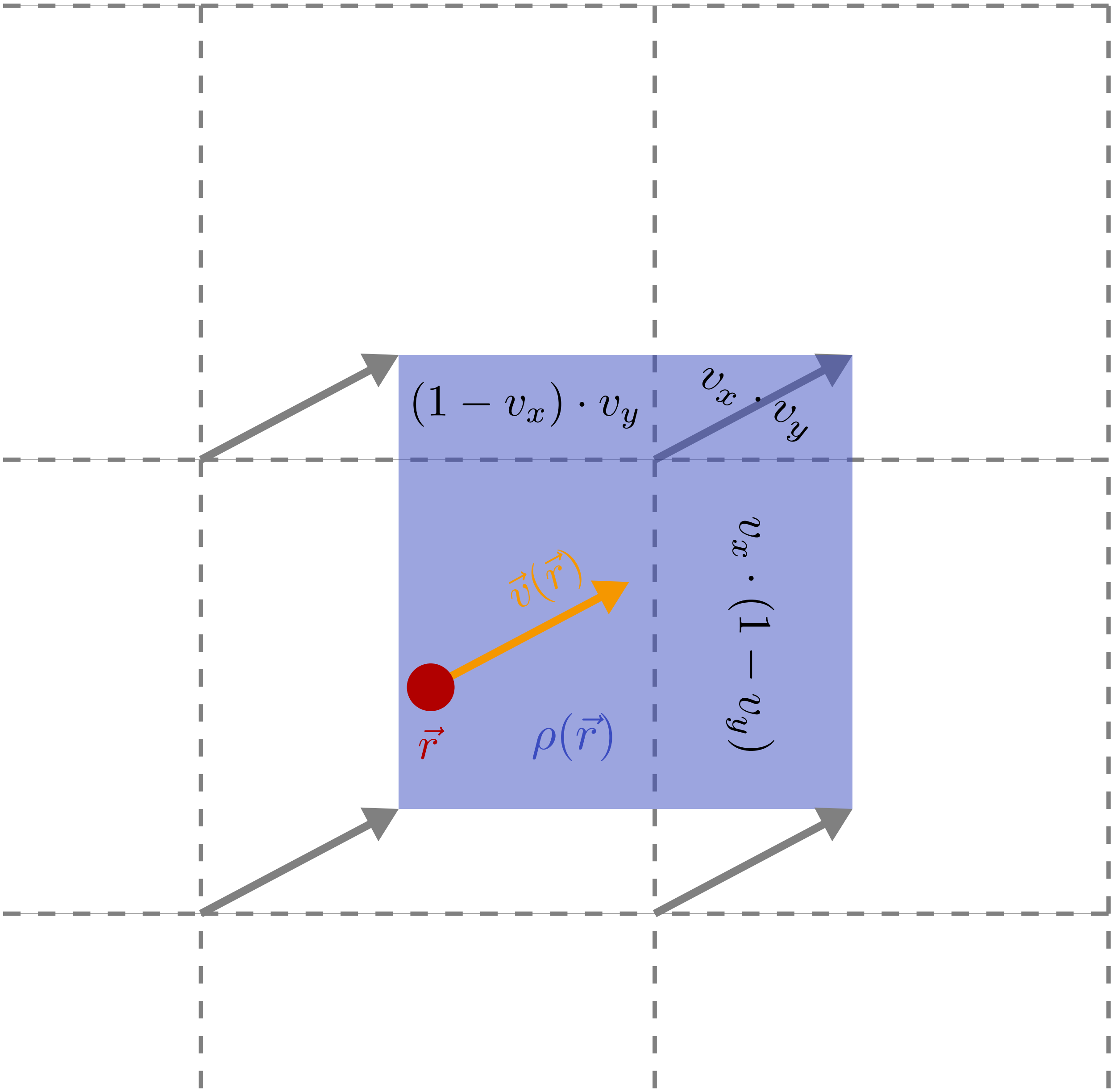

FIG. 1. Scheme for the advection on a two dimensional grid with spacing a. The dashed lines indicate the boundaries between cells with the lattice nodes in their centre. The flux to the right neighbour would be given by $n(\vec{r})v_x(1 - v_y)\frac{a^2}{\Delta t}$. Image taken from ref. 32.

because we know the statistical properties of the noise field $\eta_k(\vec{x} + \frac{\vec{a_i}}{2}, t)$ from equation 26, we can rewrite is using a Gaußian white noise $\vec{\mathcal{W}}$ as

$$\vec{\eta}_k(\vec{x}, t) = \sqrt{2D}\vec{\mathcal{W}}(t) \tag{36}$$

We use an explicit first order time stepping scheme and consider that the time integral over the white noise is $\int_t^{t+\Delta t} \vec{\mathcal{W}}(t')dt' = \sqrt{\Delta t}\vec{\mathcal{W}}(t)$, which yields

$$n_k(\vec{x}, t + \Delta t) = n_k(\vec{x}, t) - \Delta t \vec{\nabla} \cdot (\vec{j}_k^{\text{pot}}(\vec{x}, t) + \vec{j}_k^{\text{diff}}(\vec{x}, t) + \frac{1}{\sqrt{\Delta t}} \vec{j}_k^{\text{fluc}}(\vec{x}, t)). \qquad (37)$$

Applying the discretization of the flux gradient (equation 30) to the fluctuation flux we need to normalize the variance of the flux and not the flux itself. This, however, leads to the length scaling factor a_i and the stencil factor A_0 to appear under the square root

$$\vec{\nabla} \cdot \vec{j}_k^{\text{fluc}}(\vec{x}, t) \approx \sum_{i=1}^{q} \frac{1}{\sqrt{a_i A_0}} (j_{k,i}^{\text{fluc}}(\vec{x} + \frac{\vec{a}_i}{2}, t) - j_{k,i}^{\text{fluc}}(\vec{x} - \frac{\vec{a}_i}{2}, t)). \qquad (38)$$

The reaction equation (12) can be discretized by integrating over one cell [33]:

$$R_k(\vec{x}, t) = s_k K \prod_i n_i(\vec{x}, t)^{\alpha_i}. \qquad (39)$$

This is treated as a source term to the density, which yields

$$n_k(\vec{x}, t + \Delta t) = n_k(\vec{x}, t) + \Delta t R_k(\vec{x}, t). \qquad (40)$$

IV. IMPLEMENTATION

In practice, the model is implemented by coupling three solvers: a finite-volume solver for the diffusion-advection equation [1, 34], a Fourier-based solver for obtaining the electrostatic potential from the charge distribution via the Poisson equation [34], and a lattice Boltzmann hydrodynamic implementation. The simulation package ESPResSo [29, 35] contains all necessary components. As they are largely based on regular grids and matrix-vector operations, all algorithms are well suited for acceleration on graphics processors (GPUs). ESPResSo hence contains such accelerated versions [34, 36].

For educational purposes, we also provide an implementation written in Python for the advection-diffusion and for the Poisson solver in this contribution. They can be used to validate the model, but can also easily be extended for other purposes. We use the pystencils package as backend for the finite volume diffusion advection solver, and NumPy/SciPy for a Fourier-based Poisson solver. The Fourier-approach is highly efficient and requires very little custom code, but in its simple form only works in conjunction with periodic boundary conditions. This limitation is not present for the solver included with ESPResSo. While the discretization is performed manually in ESPResSo's implementation, this is largely automated by pystencils.

The full algorithm, including electrokinetics, reactions and lattice Boltzmann involves the following steps

1. Calculate total charge from per species densities and valencies
2. Obtain the electrostatic potential for the charge distribution by solving the Poisson equation via the Fourier solver
3. Calculate the fluxes, including thermal fluctuations, using Eq.29
4. Based on the fluxes, add external forces to the coupled lattice Boltzmann fluid (Eq.9)
5. Add sources and sinks to the fluxes based on chemical reactions (Eq.12)
6. Enforce any boundary conditions on the densities and fluxes
7. Solve the continuity equation (2)
8. Propagate the lattice Boltzmann fluid by one step
9. Advect the densities according to the lattice Boltzmann fluid's velocities. This is done using the volume of fluid approach, more formally known as *corner-transport upwind scheme* [1, 37].

V. VALIDATION

In this section, we demonstrate the validity of our implementations using several scenarios for which the results are either known analytically or can be obtained using an independent approach.

Fig. 2 shows the concentration profile of two species in a slit pore system. On one wall the conversion of species A to species B is being catalysed, while the reverse happens on the other side. Solving this source-drain-diffusion system yields a linear density profile for the steady-state solution:

$$n_A(x) = -\frac{2 \cdot n_0}{d \cdot D \cdot \left(\frac{1}{k_A} + \frac{1}{k_B}\right)} \left(x + \frac{d}{2} + \frac{D}{k_A}\right) \tag{41}$$

where n_0 is the initial density, d the width of the slit pore, D the diffusion constant, and k_A and k_B are the reaction rates of the reaction $A \to B$ and $B \to A$.

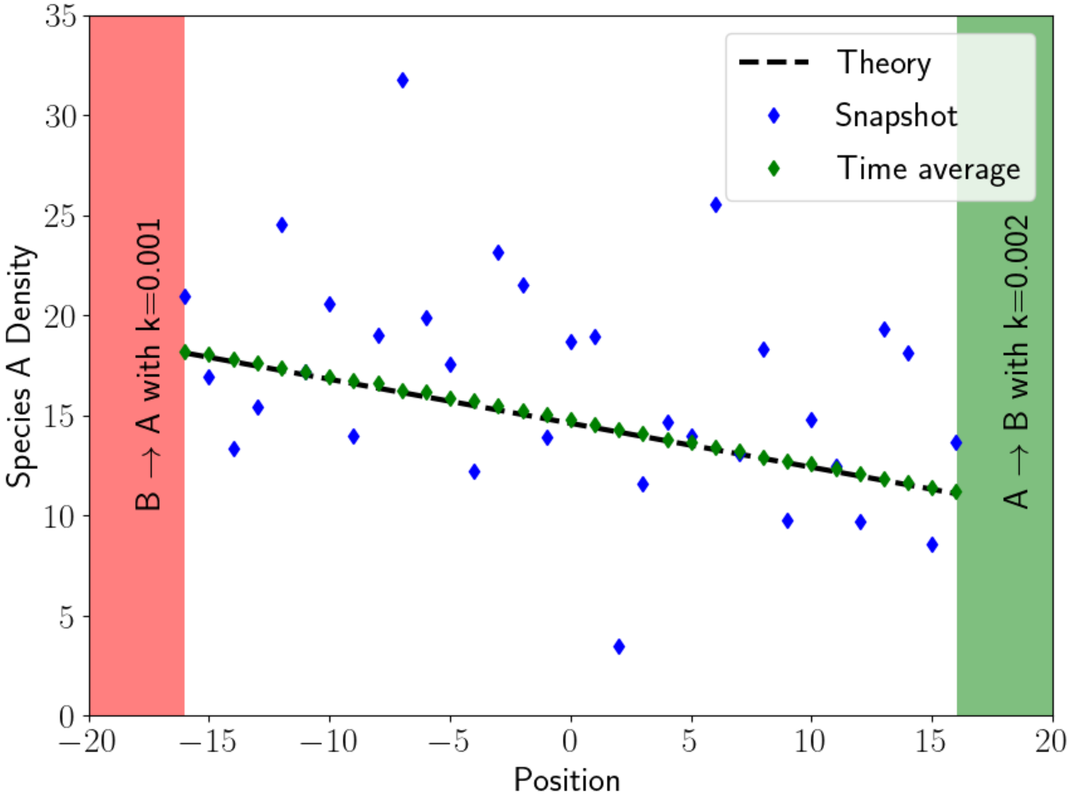

FIG. 2. Density distribution of a slit pore system, where on either side the opposite reaction takes place. While the fluctuations inflict a significant noise on the density profile of a singe time step (blue), averaging over 10000 uncorrelated snap shots (green) yields to a good approximation the theoretical predictions (black).

A. Ideal gas and Coulomb gas density distribution

Let us now turn to situations, where thermal fluctuations are of importance. To acertain that the fluctuation model has the correct physical behavior we calculate the density distribution of an ideal gas. To this end we take a system of N non-interacting particles contained in a volume V. The probability that a sub-volume $v \subset V$ encloses n particles is given by:

$$P(n) = \binom{N}{n} \left(\frac{v}{V}\right)^n \left(\frac{V-v}{V}\right)^{N-n}. \qquad (42)$$

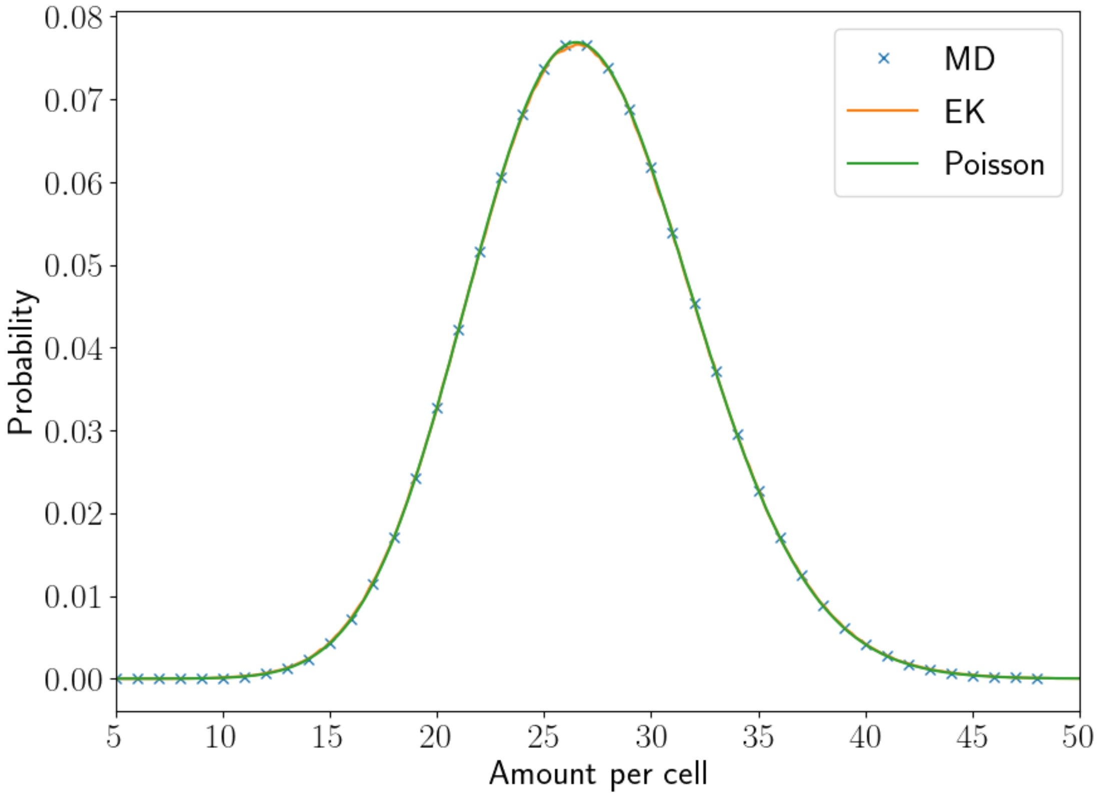

FIG. 3. Comparison of the density histogram of an ideal gas for a fluctuating electrokinetic simulation (orange), a MD simulation (blue) and the predicted theoretical distribution (green).

In the limit of $N \to \infty$ and $v \ll V$ this equation simplifies to the Poisson distribution

$$P(n) = \frac{\bar{n}^n e^{-\bar{n}}}{n!}, \tag{43}$$

where $\bar{n} = N\frac{v}{V}$. We compare the simulation data obtained from the fluctuating electrokinetic model against this equation. Additionally, we also obtained the density histogram from a molecular dynamics simulation of non-interacting particles based on the Langevin equation. The results are displayed in figure 3.

Next, we demonstrate that the electrostatic solver works in conjunction with thermal fluctuations. To this end, we examine the density histogram of a Coulomb gas containing an equal amount of positively and negatively charged ions. Since an analytical prediction is not available, we compared the electrokinetic simulation against a molecular dynamics simulation of charged particles. In the MD simulation, the charges have to be prevented

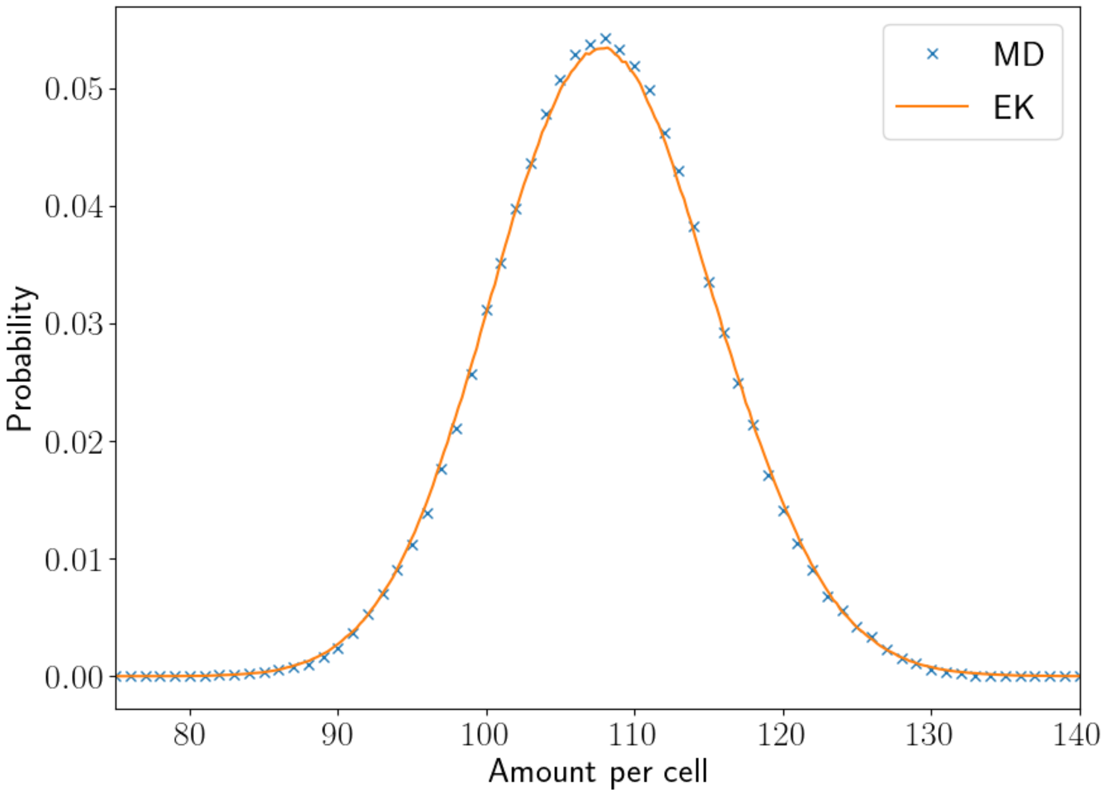

FIG. 4. Comparison of the density histogram for a Coulomb gas for the fluctuating electrokinetic simulation (orange) and the MD simulation (blue)

from coming too close to each other. This is accomplished using a hard-sphere like Weeks-Chandler-Anderson potential [38]. The results of those simulation can be observed in figure 4.

B. Effect of thermal fluctuations on the reaction rate

While the fluctuations do not change the equilibrium state of a system, they can have an influence on the dynamics of more complex systems. As an example we discuss the case for a reactive system, where the reaction rate is not linearly dependent on the concentration of the species. In other words, the reaction order is not equal to one. This can be the case, e.g, for multi-component reactions.

Let us look at the reaction of

$$2A \to B \tag{44}$$

We can then define the rate equation to be

$$\frac{\mathrm{d}\rho_B(t)}{\mathrm{d}t} = -\frac{1}{2}\frac{\mathrm{d}\rho_A(t)}{\mathrm{d}t} = k\rho_A(t)^2, \tag{45}$$

where k is the reaction rate constant. With the initial concentration of $\rho_A(0) = \rho_0$ and $\rho_B(0) = 0$, the product density turns out to be

$$\rho_B(t) = \frac{\rho_0}{2}\left(1 - \frac{1}{2kt\rho_0 + 1}\right). \tag{46}$$

However, when fluctuations are in place, the density dependent term $\rho_A(t)^2$ of equation 45 needs to be replaced by its expectation value $\langle \rho_A(t)^2 \rangle$. Under the assumption that, at any time during the reaction, ρ_A is distributed as in an ideal gas, and approximating the Poisson distribution (Eq.43) with a Gaussian distribution with mean $\langle \rho_A \rangle$ and variance $\sqrt{\langle \rho_a \rangle}$, the expectation value is given by

$$\langle \rho_A^2 \rangle = \langle \rho_a \rangle^2 + \langle \rho_A \rangle. \tag{47}$$

Inserting this into Eq.45 and solving the ODE yields a product density of

$$\widetilde{\rho}_B(t) = \frac{\rho_0}{2}\left(1 - \frac{1}{\mathrm{e}^{2kt}\left(\rho_0 + 1\right) - \rho_0}\right). \tag{48}$$

A plot of those product densities is displayed in figure 5. It can be seen that the simulations reproduce the theoretical predictions.

C. Reaction-advection-diffusion with fluctuations

To demonstrate that all of the afore mentioned algorithms can be applied together, we have set-up a model reaction-advection-diffusion system. It consists of a channel system in which the reaction $2A + B \to C$ takes place. We divided the inlet of the substrates in 3 equal parts. The upper and lower one are used for injecting species A, and in the middle part of the channel species B is entering.

The fluid advects the species through the channel, and the diffusion leads to a broadening of the density profile while the substrates move along the channel. In the increasing overlapping areas of species A and B the reaction can take place and the product C is created. The fluctuations add noise to all 3 density profiles. An image of this system is displayed in figure 6.

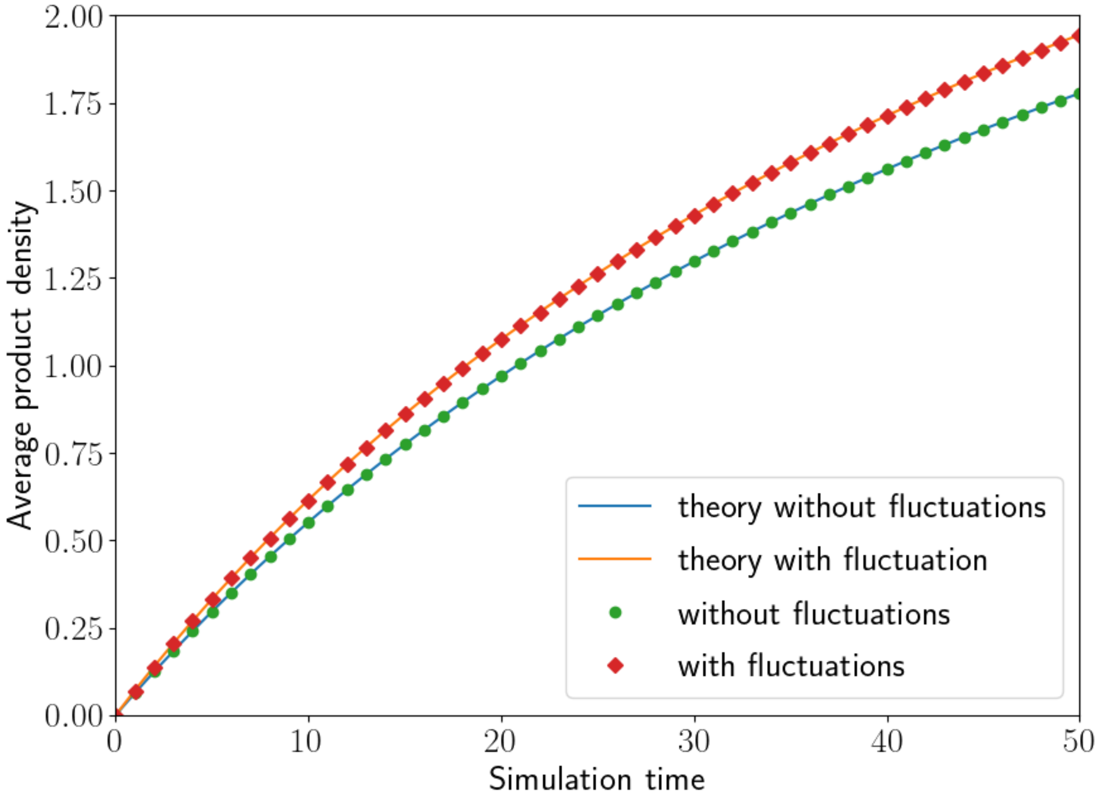

FIG. 5. Reaction product density plotted over time. The reaction was of the type $2A \rightarrow B$, where the reaction rate was set to be $r = k[A]^2$. The initial density was set to be $\rho_A(0) = 8$. The theory curves are from equations 46 and 48.

VI. CONCLUSION AND OUTLOOK

Fluctuations play an important role in many dynamical processes on the nanoscale, so any consistent physical description of reaction-advection-diffusion systems should include thermal fluctuations. We discussed in this article how to combine mesh-based solvers for thermalized electrokinetics, chemical reactions, and fluctuating hydrodynamics. Apart from the physical consistency, we demonstrated that thermal fluctuations need to be added to the electrokinetic solver to correctly reproduce the chemical reactions rates when the reaction order is not unity. Furthermore, when using an unthermalized electrokinetic model coupled to a thermalized lattice Boltzmann solver, the thermal energy of the lattice Boltzmann fluid would be depleted by the unthermalized electrokinetic solver. A similar depletion can be

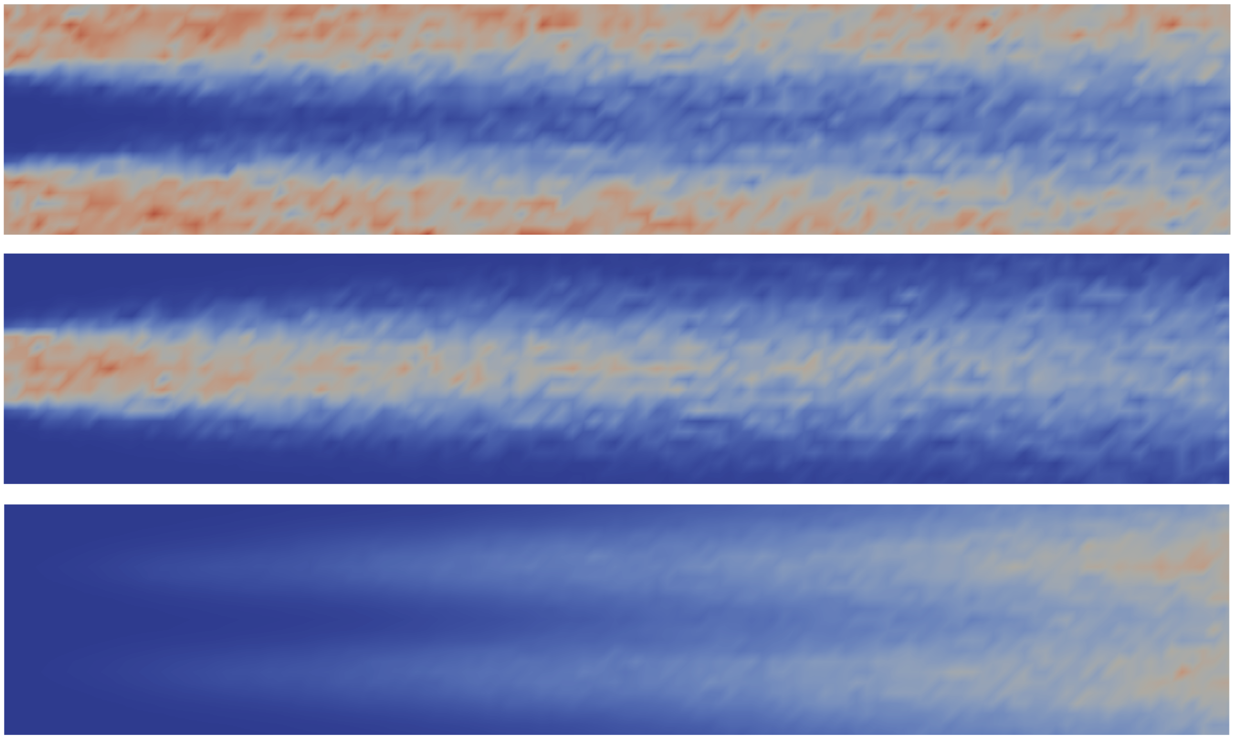

FIG. 6. Educt and product densities in a channel with fluid driving them from left to right. The reaction taking place has the form $2A + B \rightarrow C$. The upper image shows the density of species A, the middle one that of species B and the bottom one is the product density C. As inlet and outlet boundary conditions we used constant density and velocity boundary condition.

expected when a thermalized molecular dynamics simulation is coupled to an unthermalized electrokinetic or hydrodynamic solver.

We furthermore described two implementations of the reaction-advection-diffusion algorithms. One consists of manually written GPU solvers that are included as part of the simulation package ESPResSo. A second implementation is based on automatic code generation using pystencils and lbmpy, and is provided as a jupyter notebook together with this publication as supplementary material. This can be used for research scenarios in various charged soft matter problems or reactive flow problems. In particular, we intend to apply this method to catalytic systems in mesoporous material, where the transport and diffusion of the reactants towards and away from a catalyst can be studied.

ACKNOWLEDGEMENT

This work was funded by the German Research Foundation (DFG) via Project-ID 358283783 – SFB 1333 and the cluster of excellence EXC 2075 (SimTech)– Project Number 390740016.

DATA AVAILABILITY

The data that support the findings of this study will be openly available in DaRUS - Uni Stuttgart.

[1] F. Capuani, I. Pagonabarraga, and D. Frenkel, The Journal of Chemical Physics **121**, 973 (2004).

[2] G. R. McNamara and G. Zanetti, Physical Review Letters **61**, 2332 (1988).

[3] X. He and L.-S. Luo, Physical Review E **56**, 6811 (1997).

[4] T. Krüger, H. Kusumaatmaja, A. Kuzmin, O. Shardt, G. Silva, and E. M. Viggen, *The Lattice Boltzmann Method: Principles and Practice* (Springer International Publishing, Cham, 2017).

[5] I. Pagonabarraga, B. Rotenberg, and D. Frenkel, Physical Chemistry Chemical Physics **12**, 9566 (2010).

[6] B. Rotenberg and I. Pagonabarraga, Molecular Physics **111**, 827 (2013).

[7] M. Kuron, G. Rempfer, F. Schornbaum, M. Bauer, C. Godenschwager, C. Holm, and J. de Graaf, The Journal of Chemical Physics **145**, 214102 (2016).

[8] H. Daiguji, Y. Oka, and K. Shirono, Nano Letters **5**, 2274 (2005).

[9] G. Rempfer, S. Ehrhardt, N. Laohakunakorn, G. B. Davies, U. F. Keyser, C. Holm, and J. de Graaf, Langmuir **32**, 8525 (2016).

[10] G. Rempfer, S. Ehrhardt, C. Holm, and J. de Graaf, Macromolecular Theory and Simulations **26**, 1600051 (2017).

[11] N. Rivas, S. Frijters, I. Pagonabarraga, and J. Harting, The Journal of Chemical Physics **148**, 144101 (2018).

[12] C. Kim, A. Nonaka, J. B. Bell, A. L. Garcia, and A. Donev, The Journal of Chemical Physics **149**, 084113 (2018).

[13] S. Molins, D. Trebotich, C. I. Steefel, and C. Shen, Water Resources Research **48** (2012), 10.1029/2011wr011404.

[14] J. de Graaf, G. Rempfer, and C. Holm, IEEE Transactions on NanoBioscience **14**, 272 (2015).

[15] D. A. Kessler and H. Levine, Nature **394**, 556 (1998).

[16] A. Lemarchand and B. Nowakowski, EPL (Europhysics Letters) **94**, 48004 (2011).

[17] A. K. Bhattacharjee, K. Balakrishnan, A. L. Garcia, J. B. Bell, and A. Donev, The Journal of Chemical Physics **142**, 224107 (2015).

[18] D. Fange and J. Elf, PLoS Computational Biology **2**, e80 (2006).

[19] A. Donev, J. B. Bell, A. de la Fuente, and A. L. Garcia, Journal of Statistical Mechanics: Theory and Experiment **2011**, P06014 (2011).

[20] A. Donev, A. Nonaka, Y. Sun, T. Fai, A. Garcia, and J. Bell, Communications in Applied Mathematics and Computational Science **9**, 47 (2014).

[21] C. Kim, A. Nonaka, J. B. Bell, A. L. Garcia, and A. Donev, The Journal of Chemical Physics **146**, 124110 (2017).

[22] B. Dünweg, U. D. Schiller, and A. J. C. Ladd, Physical Review E **76**, 36704 (2007).

[23] B. Dünweg, U. D. Schiller, and A. J. C. Ladd, Computer Physics Communications **180**, 605 (2009).

[24] D. S. Dean, Journal of Physics A **29**, L613 (1996).

[25] M. Deng, F. Tushar, L. Bravo, A. Ghoshal, G. Karniadakis, and Z. Li, arXiv preprint arXiv:2107.05733 (2021).

[26] D. R. Ladiges, A. Nonaka, K. Klymko, G. C. Moore, J. B. Bell, S. P. Carney, A. L. Garcia, S. R. Natesh, and A. Donev, Physical Review Fluids **6** (2021), 10.1103/physrevfluids.6.044309.

[27] M. Bauer, J. Hötzer, D. Ernst, J. Hammer, M. Seiz, H. Hierl, J. Hönig, H. Köstler, G. Wellein, B. Nestler, and U. Rüde, in *Proceedings of the International Conference for High Performance Computing, Networking, Storage and Analysis* (Association for Computing Machinery, New York, 2019).

[28] M. Bauer, H. Köstler, and U. Rüde, Journal of Computational Science **49**, 101269 (2021).

[29] F. Weik, R. Weeber, K. Szuttor, K. Breitsprecher, J. de Graaf, M. Kuron, J. Landsgesell, H. Menke, D. Sean, and C. Holm, European Physical Journal Special Topics **227**, 1789 (2019).

[30] D. Röhm and A. Arnold, European Physical Journal Special Topics **210**, 89 (2012).

[31] B. Øksendal, *Stochastic Differential Equations* (Springer Berlin Heidelberg, 2003).

[32] G. Rempfer, *A Lattice based Model for Electrokinetics*, Master's thesis, University of Stuttgart (2013).

[33] J. H. M. ten Thije Boonkkamp and M. J. H. Anthonissen, Journal of Scientific Computing **46**, 47 (2010).

[34] G. Rempfer, G. B. Davies, C. Holm, and J. de Graaf, The Journal of Chemical Physics **145**, 044901 (2016).

[35] H. J. Limbach, A. Arnold, B. A. Mann, and C. Holm, Computer Physics Communications **174**, 704 (2006).

[36] D. Röhm, K. Kratzer, and A. Arnold, in *High Performance Computing in Science and Engineering '13*, edited by W. E. Nagel, D. H. Kroener, and M. M. Resch (Springer International Publishing, 2013) pp. 33–52.

[37] P. Colella, Journal of Computational Physics **87**, 171 (1990).

[38] J. D. Weeks, D. Chandler, and H. C. Andersen, The Journal of Chemical Physics **54**, 5237 (1971).